2018 IEEE Transportation Electrification Conference and Expo, Asia-Pacific (ITEC Asia-Pacific)

Estimating Lithium-ion Battery State of Charge and Health with Ultrasonic Guided Waves Using an Efficient Matching Pursuit Technique

Purim Ladpli[a†], Chen Liu[a], Fotis Kopsaftopoulos[b], and Fu-Kuo Chang[a]
[a]Department of Aeronautics and Astronautics, Stanford University, Stanford, CA, United States
[b]Department of Mechanical, Aerospace and Nuclear Engineering, Rensselaer Polytechnic Institute, Troy, NY, United States
E-mail: [†]pladpli@stanford.edu

***Abstract*— This paper presents a novel guided-wave-based framework for estimating state of charge (SoC) and state of health (SoH) of lithium-ion (Li-ion) batteries. The guided waves are propagated and sensed using low-profile, surface-mounted piezoelectric transducers on off-the-shelf Li-ion pouch cells. Special emphasis is given to the development of an efficient feature extraction strategy based on the Matching Pursuit (MP) technique. The proposed method decomposes complex waveforms into constituent 'atoms', allowing the time-frequency information of the signals to be mined. The descriptive parameters of the decomposed atoms can be extracted to show strong and meaningful correlations with SoC and SoH. Statistical prediction models for estimating SoC/SoH are built using the atom parameters as predictive features in conjunction with the traditional voltage data. It is shown that the atom parameters can augment the voltage data and statistically improve the prediction of SoC by two-fold and, in particular, of SoH by twenty-fold. The results signify the importance of encapsulating proper signal processing and feature extraction into future guided-wave-based SoC/SoH prediction frameworks.**

***Keywords*— state of charge, state of health, ultrasonic guided waves, matching pursuit, feature extraction**

I. INTRODUCTION

Electric vehicle (EV) energy storage, particularly lithium-ion (Li-ion) batteries, are extremely complex systems with a very narrow operating range and are prone to premature, unexpected failure. Optimizing battery performance, lifespan, and most importantly, safety requires continuous, accurate monitoring of the battery state of charge (SoC) and state of health (SoH) [1]. However, relying only on the terminal voltage measurement, on-board battery management systems (BMSs) still critically lack a breakthrough technique for directly probing the physical properties of the batteries to help accurately estimate SoC and SoH [1]. BMS research seems to forgo the fact that as Li-ion batteries cycle and age, their electrochemical processes are closely intertwined with mechanical evolution of the electrodes – particularly the distribution and redistribution of their mass densities and moduli [2]. Even though characterization tools for measuring these mechanical quantities are widely utilized in a laboratory setting, most of such techniques cannot be performed on vehicle-scale batteries and cannot be readily implemented in on-board BMSs due to the equipment's complexity and size [2].

Recently, acousto-ultrasonic wave propagation has started to gain interest in the research community potentially as an auxiliary, or even as an alternate, on-board method to probe a battery's mechanical behavior and ultimately improve the estimation of SoC and SoH [3-7]. Most of earlier research efforts focus on applying through-thickness compression waves by using laboratory ultrasonic probes or large piezoelectric transducers [3-5, 7]. The energy of the waves is concentrated to allow them to transmit across interfaces between electrode layers and propagate in the direction perpendicular to the laminate, enabling the localized region immediately underneath the probe to be examined. In contrast, we recently proposed a guided-wave-based technique wherein the stress waves take advantage of the geometric boundaries of the batteries to 'guide' wave propagation [6]. Using low-profile, surface-mounted piezoelectric transducers, this technique is not only more robust to variations in boundary conditions and operator errors, but also allows the waves to cover larger propagation distances and areas with minimal loss in energy.

Although promising results are demonstrated from both research thrusts, a handful of work has been done on expanding the concept towards practical, field-deployable SoC/SoH prediction. Davies et al. demonstrate that a library of time-domain parameters of the compression waves (namely, time of flight and signal amplitude) may be created from similar batteries, and then a regression model can be built to predict SoC of an independent cell [3]. However, to obtain a satisfactory accuracy level with SoH, they show that the complete waveform (data at all sampled times during a ~10μs window, or as many as ~500 predictors) is needed. The large dimensionality of predictors may require prediction models with model structures that are too computationally expensive for on-board BMSs. Our previous companion work similarly shows that time of flight and signal amplitude of guided waves may serve as accurate predictors for SoC, as well as SoH, owing to guided waves' good signal integrity against noise and boundary condition variations [6]. Furthermore, we also use multiple transducers in a network configuration and pool data from multiple propagation paths to greatly reduce the SoC/SoH prediction error.

978-1-5386-5782-9/18/$31.00 ©2018 IEEE

in the Proceedings of the 2018 IEEE Transportation Electrification Conference and Expo Asia-Pacific (ITEC Asia-Pacific)
June 6-9, 2018, Bangkok, Thailand

Nevertheless, neither effort has yet taken advantage of the rich information contained in the dynamic, non-stationary nature of pulse ultrasonic waveforms [3, 6]. Therefore, building upon our previous work, this study aims to develop a signal processing and feature extraction framework to exploit the feature-rich nature of guided waves in the context of practical SoC/SoH prediction. Signal processing and feature extraction of guided wave signals have long been a topic of research in the non-destructive testing (NDT) and structural health monitoring (SHM) community [8]. For NDT/SHM, time-frequency representation (TFR) techniques are often used to project non-stationary guided wave signals onto a time-frequency plane, from which individual, localized wave components may be extracted to be used as predictors for structural damage. Herein, with reference to SoC/SoH prediction, we develop the proposed framework based on a class of TFR, the Matching Pursuit (MP) decomposition, which allows complex guided wave signals to be efficiently decomposed into a combination of simpler, localized atoms [9]. We then show via statistical analysis that the coefficients describing these atoms are strongly correlated with battery cycling and aging behavior and can be used as effective predictors for SoC and SoH. The obtained results from this study form the basis for systematically and practically applying the acousto-ultrasonic technique towards the SoC/SoH prediction in on-board EV BMSs.

II. Problem Statement and Method of Approach

Within the context of this paper, we consider pitch-catch guided wave data from indicative commercial Li-ion pouch cells with pre-determined transducer configurations (Fig. 1). This serves as our problem setup to develop an efficient strategy to process the complex guided wave signals and extract predictive features that can lend themselves to enhancing SoC/SoH prediction. The obtained results can then be generalized and scaled into a unified framework towards other battery/transducer configurations, operating conditions, and prediction methodologies.

We first experimentally gather ultrasonic guided wave data at various SoC and SoH from the indicative pouch cells with surface-mounted piezoelectric transducers (Section III). The waveform structure and its progression due to changing SoC/SoH are studied in order postulate an appropriate MP-based TFR technique to process and project the signals onto basis functions (Section IV). Then, functional relationships between the parameters of the basis functions and the changes in SoC/SoH are established (Section V). A comparative statistical analysis is conducted to evaluate the efficacy of the proposed time-frequency feature extraction, in comparison and in conjunction with the conventional voltage measurement and time-domain features (Section VI).

III. Preliminary Experiments & Indicative Results

The experimental results, which the MP feature extraction and statistical analysis are based on, have been discussed in our previous companion work [6]. Pitch-catch guided wave propagation experiments were performed on 3,650mAh off-the-shelf Li-ion pouch batteries (graphite/NCM chemistry) (AA Portable Power Corp.) (Fig. 1). Guided wave signals were gathered at various battery SoC and SoH from surface-mounted, small-footprint piezoelectric disc transducers (6.35mm-diameter PZT-5A in the SMART Layer format; Acellent Technologies, Inc.) at the locations shown in Fig. 1. One of the piezoelectric discs can be chosen as an actuator to generate acousto-ultrasonic guided waves. The other piezoelectric disc then serves as a receiver to record the transmitted guided wave signals. The so-called "pitch-catch" experiments used five-peak Gaussian-windowed tone bursts with center frequencies between 100 to 200 kHz. The piezoelectric transducers were actuated and sensed using anultrasonic data acquisition system (ScanGenie II; Acellent Technologies, Inc.). Ultrasonic measurements were taken every 1 minute during electrical cycling.

The ultrasonic data acquisition was synchronized with a battery analyzer (BST8-3; MTI Corporation), which performed battery cycling and aging. The cells were electrically discharged at an elevated temperature of 45°C with a constant current rate of 3,000 mA from 4.2V (100% SoC) to 3.0V (0% SoC). A total of 200 discharge cycles were performed. The remaining capacity for each cycle, which is our definition of SoH, was calculated by evaluating the cycle discharge capacity normalized with respect to the value from the first cycle. The cycle-to-cycle terminal voltage of a representative cell and its capacity fading (SoH degradation) characteristics are shown in Fig. 2.

The guided wave responses could be seen to exhibit repeatable time-domain variations with changing SoC and SoH. Representative actuator-sensor waveforms from the pouch cell experiment are shown in Fig. 3. Fig. 3A shows the distinct evolution of the guided wave structure with respect to SoC within one discharge cycle. Fig. 3B, on the other hand, demonstrates the changes in the time-domain waveforms due to capacity fading (SoH degradation). These interplays between guided wave propagation and electrochemical processes were shown to be the results of the distribution and redistribution of electrodes' mechanical properties – namely, moduli and densities – during cycling and aging [6].

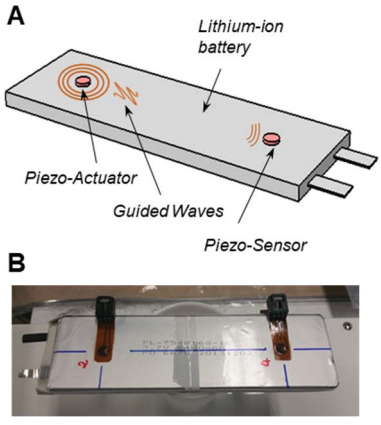

Fig. 1. A) Schematics of pitch-catch guided wave propagation. B) experimental pouch cell with built-in piezos.

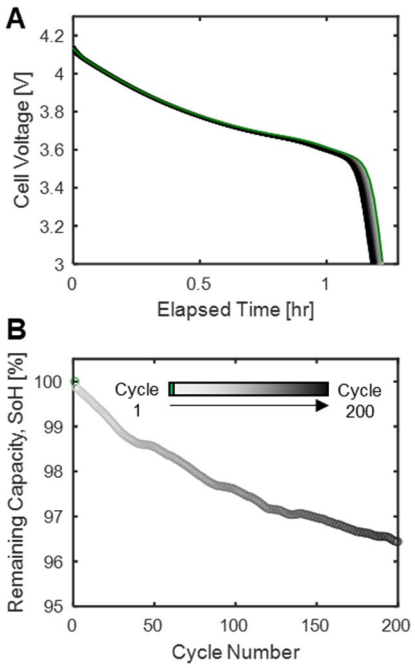

Fig. 2. A) Cycle-to-cycle terminal voltage measurement from a representative cell. B) Remaining capacity (SoH) -vs- cycle number showing the indicative capacity fading characteristics of the batteries under testing.

IV. Feature Extraction Using Matching Pursuit

In our previous work, we showed the feasibility of the guided wave method in estimating SoC/SoH by performing state prediction using only two time-domain features – i.e., time of flight and signal amplitude (ToF and SA, respectively) [6]. These limited features only represent the aggregate behavior of the time-domain waveforms. However, pitch-catch tone-burst guided wave signals are dynamic, non-stationary, and multi-dimensional (in time and frequency). This can be intuitively seen from Fig. 3 that different time-axis portions of the waveforms (wave packets) show distinct characteristics with respect to the changes in SoC and SoH. Instead, using an appropriate time-frequency representation method, numerous predictive features can be extracted from the information-rich guided wave signals. The multi-dimensional time-frequency features may be pooled with the one-dimensional voltage measurement to construct a new class of SoC/SoH prediction models. This potentially allows prediction accuracy to be significantly improved and/or greatly simplifies the structure and complexity of the prediction model.

In this current work, we propose an efficient feature-extraction algorithm based on the MP decomposition technique [9]. MP is a time-frequency representation method, which is widely used in the field of guided-wave SHM for analyzing guided wave signals with respect to the evolution of structural damage. MP finds the best matching projections of the guided wave signals onto the span of a redundant dictionary of waveforms or atoms. In essence, MP decomposes the signals into a linear combination of constituent waveforms that was found to best match the original signal structure.

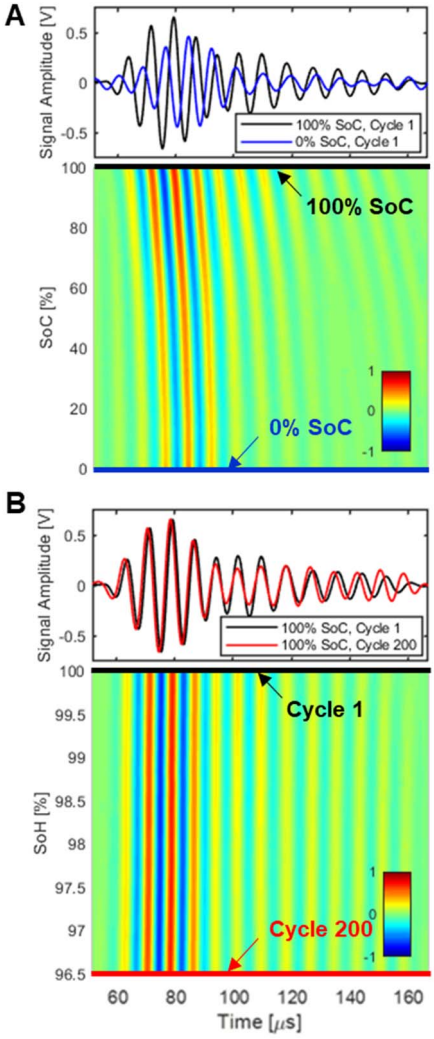

Fig. 3. Time-domain evolution of guided wave signals with respect to changes in SoC and SoH. A) Changes in the time-domain signals with respect to SoC. B) Changes in the time-domain signals with respect to SoH. Ultrasonic data from the diagonal path at 125 kHz center frequency.

We employ MP using the Gabor dictionary (a collection of scaled, translated, and modulated versions of Gaussian-windowed tone bursts) to decompose the guided wave responses into a linear expansion of constituent tone-burst atoms (Fig. 4). The Gabor functions can be represented by the following equation:

$$g(t) = e^{-\pi t^2}, \tag{1}$$

$$g_{\gamma=(s,u,v,w)}(t) = g\left(\frac{t-u}{s}\right)\cos(vt+w)$$

where the Gabor dictionary D is a collection of g_γ. γ is a set of possible Gabor parameters s, u, v, and w, which are coefficients of scaling, translation, modulation, and phase change, respectively. The dictionary thus contains all possible expected waveforms or atoms.

The Gabor dictionary is a natural choice for our application as the actuation signal used in this study is also designed to be a modulated Gaussian-windowed tone burst.

Given that the incident pulse is a Gabor function, the sensing signals can also be represented by one or a sum of Gabor functions. This adaptively accelerates the MP algorithm and allows meaningful pulses to be efficiently extracted out of noisy signals.

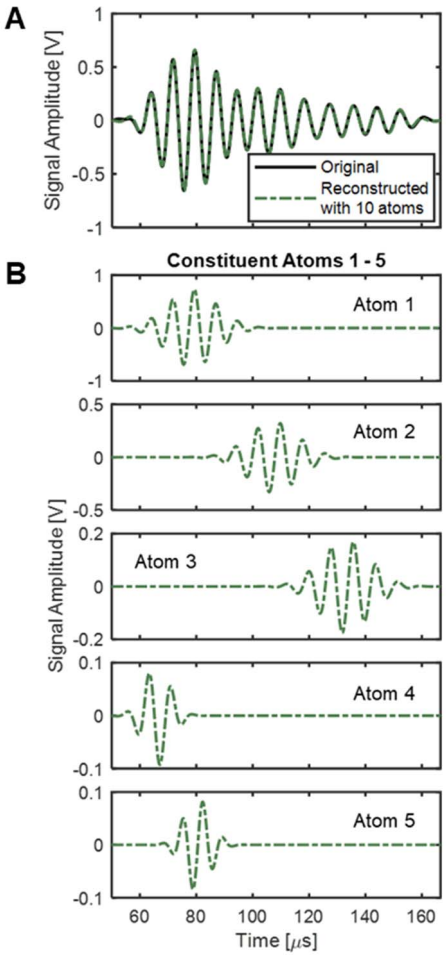

Fig. 4. Functionality of Gabor-based MP decomposition. A) Original waveform at 100% SoC and 100% SoH in comparison with the reconstructed waveform using a linear combination of the first 10 constituent Gabor atoms. B) The waveform structure of the first 5 decomposed atoms.

The MP algorithms iteratively decomposes the original waveform into K constituent atoms in the following way:

1. Free Baseline Decomposition

1.1) First-Pass Sub-Optimal Search. Let f be the original signal at baseline SoC and SoH (e.g. SoC = 100%, SoH = 100%). First, we pre-define a subspace $\Gamma(s, u, v)$, where the parameter s is selected among a uniformly distributed set of expected receiving pulse widths by considering the incident pulse width (as determined by the actuation center frequency and number of cycles); v is naturally selected to be concentrated around the center frequency of the actuation; and u is selected among the discrete sampled time. Within the pre-defined subspace Γ, the sub-optimal set γ' which represents the best atom in D can be chosen to maximize:

$$|\langle f,\, g_{\gamma'}\rangle| \tag{2}$$

The operator <., .> represents a standard vector inner product. The residual signal Rf after subtracting the component along the best atom chosen per above can be computed as:

$$Rf = f - \langle f,\, g_{\gamma'}\rangle\, g_{\gamma'} \tag{3}$$

The process is then repeated on the residual Rf and is terminated after the K^{th} iteration (after K atoms have been extracted). In this study, the first ten constituent atoms were extracted from the guided wave signals at a given SoC/SoH state (K = 10), which allows more than 95% of the original signal energy content to be captured in every case. We also employ the following transformation to encode the phase and amplitude of the Gabor atoms into two dependent variables, a_k and b_k, following the equation below [10]:

$$a_k = \langle R^k f, P_{\gamma'_k}\rangle,\;\; b_k = \langle R^k f, Q_{\gamma'_k}\rangle \tag{4}$$

$$P_{\gamma'}(t) = g\left(\frac{t-u}{s}\right)\cos(vt)\,,\;\; Q_{\gamma'}(t) = g\left(\frac{t-u}{s}\right)\sin(vt)$$

where $R^k f$ is the residual signal after k^{th} atom-decomposition iteration.

1.2) Optimal Search Based on Sub-Optimal Parameters. Note that the pre-defined sub-space in the earlier stage is a set of discrete Gabor basis functions for the sake of efficient computation. Therefore, only sub-optimal atoms are determined. Using the sub-optimal parameters γ'_k obtained earlier as the initial guess, non-linear least squares can be employed to perform a local search and determine the optimal Gabor functions [11]. The standard Gauss-Newton method is implemented to numerically search for the optimal parameters $\gamma_k = (s_k, u_k, v_k)$ in the neighborhood of the sub-optimal sets so as to minimize the energy of the residual at k$^{\text{th}}$ iteration. (a_k, b_k) are then re-calculated using the same equation above. This double-search strategy is performed at every atom-decomposition iteration. Consequently, this allows us to obtain an optimal set of parameters for the constituent atoms by performing decomposition on signals at a reference state (i.e., SoC = 100%, SoH = 100%).

2. Constrained Decomposition of Signals at Subsequent States

To address the computational expense requirements for on-board BMS applications, an efficient decomposition method is required for the conceivably large stream of data. Therefore, a constrained MP decomposition is applied wherein signals at subsequent SoC/SoH states are decomposed via MP by imposing constraints using the parameters of the preceding state (according to the time sequence of the data acquired during experiment). The shape of each atom of the subsequently analyzed signals is constrained to be similar to that of the preceding one –i.e., fixed scale and frequency $(s_k,\, v_k)_{\,k\,=\,[1,\,2,\ldots\,K]}$ – while the

amplitude and translation parameters (a_k, b_k, u_k) are allowed to change. This also ensures that the decomposition is robust against external factors such as noise and data corruption, which would have otherwise caused invalid atoms to be extracted. Only a Gauss-Newton numerical search is required to seek the optimal (a'_k, b'_k, u'_k) parameters of the subsequent signals in the vicinity of the immediately preceding sets (a_k, b_k, u_k). It is important to note that the double-search algorithm needs to be performed once for the initial state (SoC = 100%, SoH = 100%). The subsequent data points only require the computationally lighter constrained decomposition. We then monitor the evolution of (a_k, b_k, u_k) with reference to changing SoC and SoH.

V. Evolution of Gabor Parameters with SoC/SoH

The changes in the guided wave signals with respect to SoC become more apparent when their constituent atoms are individually observed. Fig. 5A shows the changes in the original guided wave signals and their first three constituent Gabor atoms at two SoC (100% and 0%) from the first discharge cycle (SoH = 100%). It is worth noting that MP is able to decompose the entire complicated original waveform into localized and more defined tone bursts, which are centered at different points along the time axis. Each portion of the original waveform can now be analyzed separately by considering the evolution of the constituent Gabor atoms with respect to varying SoC.

The first atom, which represents the direct-path waveform and thus containing the majority of the energy content, shows the expected behavior of decreasing SA and increasing ToF at lower SoC. The behavior is reminiscent of the decrease in the aggregate modulus to mass density ratio with decreasing SoC, which results in decreasing propagation speeds and higher attenuation. The following atoms are known to originate from secondary wave modes that travel at different speeds, boundary reflections, and scattered signals from interlaminar surfaces. While there are meaningful and strong correlations between these secondary atoms and SoC, their physical interpretation is subject of ongoing work. The analysis of these complex waveforms requires high-fidelity computational modelling of wave propagation. Nevertheless, the essence of this work is captured: MP with the Gabor dictionary is capable of extracting waveform compositions that are strongly correlated with battery SoC.

The correlations between the Gabor atoms and SoC can be phrased in a way that is useful for SoC prediction by considering the functional relationships between the Gabor parameters (a_k, b_k, u_k) and SoC. These functional relationships for the first three atoms are plotted in Fig. 5B showing (a_k, b_k, u_k) as a function of SoC. The overall trends of (a_k, b_k, u_k) agree with the time-domain observations at varying SoC as presented above. Additionally, the (a_k, b_k, u_k) trends also capture the non-linearity driven by intercalations and phase transitions at various stages along the discharge process. The correlations between (a_k, b_k, u_k) and SoC established through these functional relationships suggest that the Gabor parameters may be utilized in a collective fashion to aid the prediction of SoC.

Independently of SoC, strong correlations between guided wave signals and SoH can also be seen in the extracted Gabor atoms as shown in Fig. 6A. The first three atoms are plotted to show the time-domain shifts in the waveform after 200 discharge cycles (SoH degraded to 96.5%) despite the same SoC of 100%. Similarly, functional relationships between the Gabor parameters (a_k, b_k, u_k) and SoH can be established at any given SoC as illustrated in Fig. 6B. Comparing to the terminal cell voltage, which is minimally perturbed by aging (Fig. 2A), the Gabor parameters show a significantly larger net change with respect to the change in SoH. Therefore, besides presenting more features to the SoH prediction, the greater magnitude of the effects from the Gabor parameters (relative to the variance of the variables themselves) may effectively contribute to improving prediction accuracy.

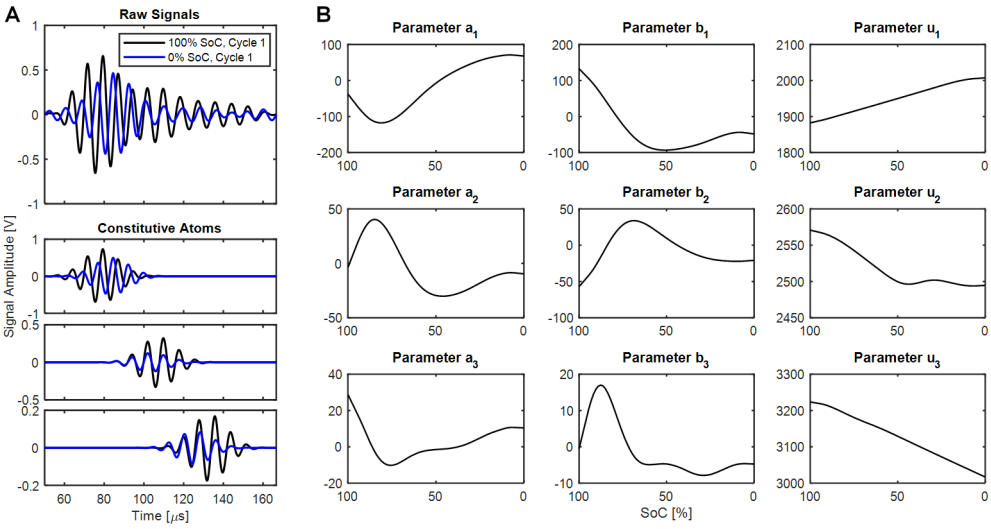

Fig. 5. *Behavior of Gabor atoms due to the changes in SoC. A) Time-domain behavior of the first three constituent atoms with respect to SoC during Cycle 1 (SoH = 100%). B) The extracted (a_k, b_k, u_k) from the first three atoms and their functional relationships with respect to SoC.*

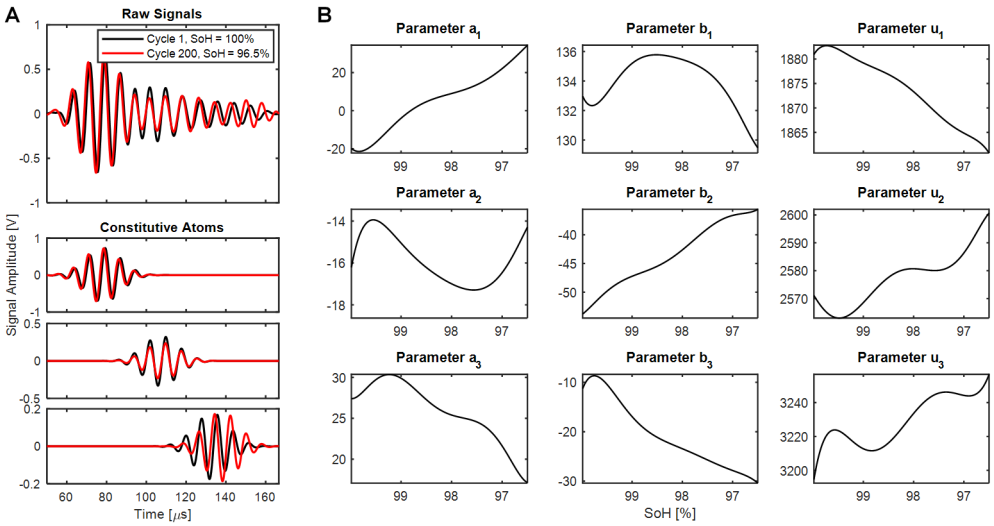

Fig. 6. *Behavior of Gabor atoms due to the changes in SoH. A) Time-domain behavior of the first three constituent atoms with respect to SoH while holding SoC constant at 100%. B) The extracted (a_k, b_k, u_k) from the first three atoms and their functional relationships with respect to SoH.*

The effects on the Gabor parameters due to changes in SoC and SoH as observed independently can be combined to form a basis for the multivariate SoC/SoH prediction. The Gabor parameters that encompass the entire range of SoC and SoH within this experiment are analyzed collectively, and these results are shown in Fig. 7. The surface plots are the loci of extracted Gabor parameters at a given pair of state variables: SoC and SoH. In other words, the Gabor parameters can be expressed explicitly as functions of both SoC and SoH. This illustrates the possibility of creating a framework to use the Gabor parameters as predictive features in an inverse setting to simultaneously estimate battery SoC and SoH.

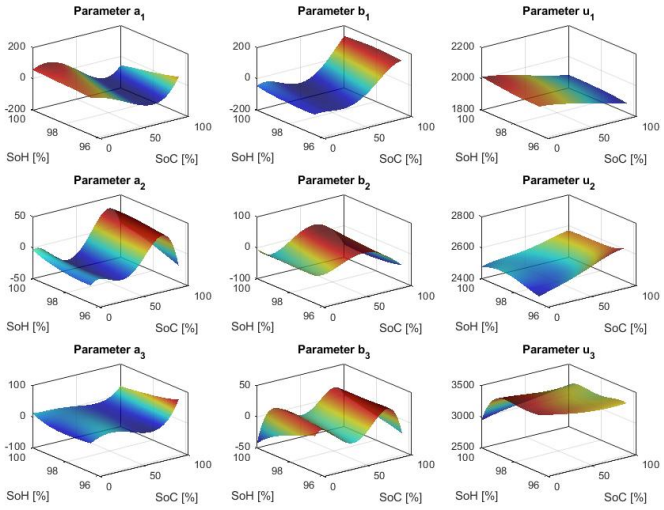

Fig. 7. *Gabor parameters of the first three atoms as a function of SoC & SoH. u_k is the translation parameter. a_k and b_k are coefficient of the sine and cosine terms in the Gabor function.*

VI. SoC/SoH Prediction Models

In this section, we perform a statistical analysis to comparatively evaluate the efficacy of Gabor parameters as predictors for SoC/SoH with reference to traditional voltage measurements and time-domain features. This first-pass statistical analysis attempts to create models that explicitly describe SoC and SoH as a function of the predictive features and evaluate the model performance by batch regression. It is important to note that this comparative evaluation is model agnostic. For practical implementation, the most appropriate model needs to be identified from a plethora of machine learning tools and state estimation techniques, with additional work in optimizing the model structure.

The prediction methods are based on Generalized Additive Models (GAMs) [12]. GAMs with regression splines, unlike other statistical learning methods, are chosen because they are easy to interpret and allow model structures of different complexity levels to be systematically compared. GAMs are a non-parametric regression technique, which allows dependent variables to be described by smooth non-linear functions of covariates. Thin-plate regression splines were employed as smoothed non-linear fits of covariates using maximum penalized likelihood to prevent overfitting. The GAM analysis uses the *'mgcv'* package (version 1.8-18) in *R*. A family of multivariate GAMs, a multivariate normal model (*multinom*), is used to fit the bivariate (SoC and SoH) response to multiple predictors. Herein, only the smooth main effects were included without interaction among predictors.

$$\begin{aligned} SoC &= \alpha_1 + f_{1,1}(X_1) + f_{1,2}(X_2) + \ldots + f_{1,P}(X_P) \\ SoH &= \alpha_2 + f_{2,1}(X_1) + f_{2,2}(X_2) + \ldots + f_{2,P}(X_P) \end{aligned} \quad (5)$$

where $f_{i,j}$ is the regression spline relating the response Y_i (SoC and SoH) to the predictor X_j. α_i is the zero-offset for each of the bivariate response.

Each GAM involves P predictors X_j which are a subset of predictors selected from the set of all available features (V, a_k, b_k, u_k); k = 1-10, where V is the cell terminal voltage. The different model structures analyzed in this section contain different subsets of predictors whose comparative statistical performance in predicting SoC and SoH is being evaluated. The residual maximum likelihood (REML) scores and Akaike Information Criterion (AIC) scores [85] are calculated and compared for each of the models. The fitted models are then applied to the validation dataset to compare the predicted and measured SoC and SoH. From which, the 10-fold cross validation (CV) error can be evaluated to reinforce the model comparison in addition to the use of classical statistical criteria.

VII. Comparative Statistical Results

The comparative performance of various GAM structures with different subsets of features can be seen from the CV errors of SoC and SoH prediction (root mean squared errors (RMSE)) as shown in Fig. 8. The detailed statistical results of the model structures considered in this study are summarized in TABLE I. By using Gabor parameters in conjunction with the conventional voltage measurement as predictors for SoC and SoH, the prediction accuracy is significantly improved. Using the entire set of the available features ((V, a_k, b_k, u_k); k = 1-10), the SoC prediction accuracy can be increased by almost two-fold. Particularly remarkable is the SoH prediction whereby augmenting the voltage measurement with guided-wave Gabor parameters improves prediction accuracy by as much as 20 times. It is well known that terminal voltage, while being able to serve as a strong indicator for SoC, is almost invariant with SoH. Given that this is a two-unknown problem (SoC and SoH), relying only on voltage measurement alone would intuitively result in an underdetermined system. Hence, it is imperative and demonstrated herein that additional parameters that are strongly correlated with SoH need to be taken into consideration.

Our analysis also signifies the importance of signal processing and feature extraction in using guided wave for SoC/SoH prediction. Our previous work only considered time domain parameters (ToF and SA), which are indicative of the global behavior of the waveform, or more specifically, the behavior the wave packet with the highest energy content [6]. The model that only uses the Gabor parameters from the first constituent atom ((a_k, b_k, u_k); k = 1) exhibits almost equivalent prediction performance to the time-domain-only model. This is because the first constituent Gabor atom is also by and large reminiscent of the highest energy wave packet. By using Gabor parameters from subsequently extracted atoms the SoC/SoH prediction accuracy can then be seen to precipitously improve. That is, a lot of meaningful correlations with SoC and SoH are encoded in other portions of the waveform beyond the primary wave packet, which can only be extracted via an appropriate time-frequency representation method.

Moreover, it is noteworthy that this analysis treats SoC and SoH as a bivariate response. The prediction models simultaneously estimate both SoC and SoH using pooled predictors. This is in stark contrast to our previous work and recent efforts in the literature [3, 6], where SoC and SoH are estimated independently of each other – i.e., one state is held constant or not considered when estimating the other.

Therefore, the bivariate prediction results confirm that the guided wave Gabor parameters, unlike cell voltage, have sufficiently meaningful correlations simultaneously to both SoC and SoH. Also considering that our statistical analysis was data-driven and was merely a comparative batch regression, there is room for improvement by, for instance, moving towards more efficient and robust model-based approaches. Investigation is underway to develop physics-based models that functionally relate the Gabor parameters to the SoC/SoH space. The model fidelity will also be improved by experimentally exploring and taking into account other factors such as discharge profiles, temperature, cell-to-cell variability, etc.

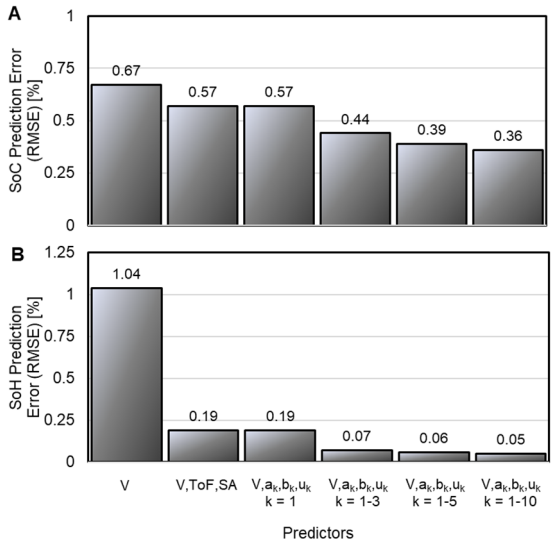

Fig. 8. *Prediction performance of different GAM structure with various subsets of predictive features. A) Average SoC prediction error (RMSE). B) Average SoH prediction error (RMSE).*

VIII. Concluding Remarks

This work established a framework for applying novel signal processing and feature extraction that enable the use of acousto-ultrasonic guided waves for battery SoC/SoH prediction. We experimentally demonstrated the SoC/SoH-induced evolution in the guided wave signals propagated through commercial Li-ion pouch batteries using low-profile, surface-mounted piezoelectric transducers. It was found that the complex interplay between electrochemical processes and wave propagation physics resulted in meaningful SoC/SoH correlations to be encoded in these dynamic, non-stationary, multi-dimensional waveforms. In this work, special emphasis was therefore given to developing an efficient time-frequency representation method to process the waveforms and extract predictive features that significantly improve the SoC/SoH predictions. In essence, this study has contributed the following:

- An efficient MP algorithm was proposed based on the Gabor dictionary to decompose complex guided wave signals into a linear combination of simpler, constituent tone-burst atoms. We also employed constrained MP decomposition that allowed guided signals at contiguous states to be efficiently and accurately decomposed by exploiting the atom information of the preceding states.
- The parameters that describe the Gabor atoms' waveform structure, or Gabor parameters, were extracted and collectively analyzed over the SoC/SoH space studied in this work. Functional relationships between the Gabor parameters and SoC/SoH showed strong and meaningful correlations which substantiated the use of the Gabor parameters as predictive features for SoC/SoH prediction.
- GAMs were generated with different model structures utilizing different subsets of the pool of predictive features. We showed that the prediction accuracy of SoC and particularly SoH was significantly improved when augmenting the conventional voltage measurement with the guided-wave Gabor parameters. We also treated SoC and SoH as a bivariate response to demonstrate that the Gabor parameters are simultaneously and strongly correlated to both SoC and SoH.

The current and future work addresses the improvement of the MP algorithm to include possible dispersion characteristics in an efficient manner by coupling data-driven decomposition with physical knowledge. Transitioning from a data-driven predictive approach to a model-based approach is also underway. This task requires a full understanding of the underlying physical phenomena that govern the SoC/SoH-induced changes in the time-frequency space of guided waves. While further investigation is needed to understand the influence of factors, such as temperature and operating profiles, the heretofore obtained results clearly show the feasibility of using guided waves for SoC/SoH prediction and lay groundwork for future studies.

ACKNOWLEDGMENTS

The work is supported by the Advanced Research Projects Agency - Energy (U.S. Department of Energy) [grant number DE-AR0000393] and the Stanford Precourt Institute of Energy. The authors highly appreciate support from Dr. Keith Kepler, Dr. Hongjian Liu, and Dr. Michael Slater at Farasis Energy, Inc., as well as Mr. Raphael Nardari at Zenith Aerospace, Inc. for feedback and suggestions. The authors would like to thank Dr. Surajit Roy at California State University, Long Beach, for valuable advice on the matching pursuit algorithms. We would also like to thank Acellent Technologies Inc. for providing necessary hardware support for the experiments conducted in this research.

REFERENCES

[1] Waag, W., Fleischer, C., and Sauer, D.U.: 'Critical review of the methods for monitoring of lithium-ion batteries in electric and hybrid vehicles', Journal of Power Sources, 2014, 258, pp. 321-339
[2] Linden, D.: 'Handbook of batteries', in Editor (Ed.)^(Eds.): 'Book Handbook of batteries' (1995, edn.), pp. 265
[3] Davies, G., Knehr, K.W., Van Tassell, B., Hodson, T., Biswas, S., Hsieh, A.G., and Steingart, D.A.: 'State of Charge and State of Health Estimation Using Electrochemical Acoustic Time of Flight Analysis', Journal of The Electrochemical Society, 2017, 164, (12), pp. A2746-A2755
[4] Gold, L., Bach, T., Virsik, W., Schmitt, A., Müller, J., Staab, T.E., and Sextl, G.: 'Probing lithium-ion batteries' state-of-charge using ultrasonic transmission–Concept and laboratory testing', Journal of Power Sources, 2017, 343, pp. 536-544
[5] Hsieh, A., Bhadra, S., Hertzberg, B., Gjeltema, P., Goy, A., Fleischer, J., and Steingart, D.: 'Electrochemical-acoustic time of flight: in operando correlation of physical dynamics with battery charge and health', Energy & environmental science, 2015, 8, (5), pp. 1569-1577
[6] Ladpli, P., Kopsaftopoulos, F., and Chang, F.-K.: 'Estimating state of charge and health of lithium-ion batteries with guided waves using built-in piezoelectric sensors/actuators', Journal of Power Sources, 2018, 384, pp. 342-354
[7] Sood, B., Osterman, M., and Pecht, M.: 'Health monitoring of lithium-ion batteries', in Product Compliance Engineering (ISPCE), 2013 IEEE Symposium on, pp. 1-6
[8] Raghavan, A.: 'Guided-wave structural health monitoring', 2007
[9] Mallat, S.G., and Zhang, Z.: 'Matching pursuits with time-frequency dictionaries', IEEE Transactions on signal processing, 1993, 41, (12), pp. 3397-3415
[10] Ferrando, S.E., Kolasa, L.A., and Kovačević, N.: 'Algorithm 820: a flexible implementation of matching pursuit for Gabor functions on the interval', ACM Transactions on Mathematical Software (TOMS), 2002, 28, (3), pp. 337-353
[11] Hong, J.-C., Sun, K.H., and Kim, Y.Y.: 'The matching pursuit approach based on the modulated Gaussian pulse for efficient guided-wave damage inspection', Smart Materials and Structures, 2005, 14, (4), pp. 548
[12] Wood, S.N.: 'Fast stable restricted maximum likelihood and marginal likelihood estimation of semiparametric generalized linear models', Journal of the Royal Statistical Society: Series B (Statistical Methodology), 2011, 73, (1), pp. 3-36

TABLE I
COMPARATIVE STATISTICAL RESULTS OF DIFFERENT GAM STRUCTURES USING GABOR PARAMETERS TOGETHER WITH CELL VOLTAGE AS PREDICTORS

	Guided wave information only					Guided wave + cell voltage					
Parameters	**Model 1**	**Model 2**	**Model 3**	**Model 4**	**Model 5**	**Model 6**	**Model 7**	**Model 8**	**Model 9**	**Model 10**	**Model 11**
Predictors	(ToF, SA)	(a_k, b_k, u_k); k = 1	(a_k, b_k, u_k); k = 1-3	(a_k, b_k, u_k); k = 1-5	(a_k, b_k, u_k); k = 1-10	(V)	(V, ToF, SA)	(V, a_k, b_k, u_k); k = 1	(V, a_k, b_k, u_k); k = 1-3	(V, a_k, b_k, u_k); k = 1-5	(V, a_k, b_k, u_k); k = 1-10
Number of predictors	2	3	9	15	30	1	3	4	10	16	31
Statistical Results											
SoC CV10 RMSE [%]	5.24	11.96	1.65	0.94	0.55	0.67	0.57	0.57	0.44	0.39	0.36
SoH CV10 RMSE [%]	0.56	0.7	0.08	0.06	0.05	1.04	0.19	0.19	0.07	0.06	0.05
REML	24426	31541	-15311	-26096	-39329	11272	-17596	-21105	-34968	-46282	-49316
AIC	48539	62685	-31443	-53347	-80615	22412	-35616	-42677	-70666	-93772	-100561